Crystallization Kinetics of Poly(ethylene oxide) in Poly(ethylene oxide)−Polystyrene−Poly(ethylene oxide) Triblock Copolymers

G. Floudas*,† and C. Tsitsilianis‡

Institute of Electronic Structure and Laser, Foundation of Research and Technology-Hellas (FORTH), P. O. Box 1527, 711 10 Heraklion Crete, Greece, Department of Chemical Engineering, University of Patras, 26500 Patras, and Institute of Chemical Engineering and High Temperature Chemical Processes, P. O. Box 1414, 26500 Patras, Greece

Received October 30, 1996; Revised Manuscript Received February 5, 1997[⊗]

ABSTRACT: The structure and crystallization kinetics of poly(ethylene oxide) (PEO) in the homopolymer and in two triblock copolymers of poly(ethylene oxide)−polystyrene−poly(ethylene oxide) (PEO−PS−PEO), crystallized from the ordered melt, have been studied respectively with X-ray diffraction, optical microscopy and differential scanning calorimetry, rheology. A multilayer lamellar structure with a spherulitic superstructure is formed by the crystallizable block, and the amorphous phase is incorporated in the interlamellar PEO regions. The amorphous midblock exerts no influence on the local structure of PEO but has a strong influence on (i) the crystallinity, (ii) the equilibrium melting temperature, and (iii) the thickness of PEO domains. Crystallization proceeds via nucleation and growth and is faster in the triblocks under conditions of equal supercooling. Shear has a pronounced effect on the shape of the crystallization process but little effect on the average times of crystallization. It is shown here that rheology can be used to obtain the *equilibrium* melting temperature in semicrystalline polymers.

Introduction

Block copolymers composed of crystalline and amorphous blocks are interesting materials to study the crystal structure, morphology, crystallization kinetics, and dynamics. The reason is that the covalent bonding of the two chemically dissimilar blocks, composed from amorphous and crystalline segments, results in a new material whose properties are not a simple function of the indivintual homopolymers. For example, the lamellar thickness in the crystalline phase is a function of the degrees of polymerization of both blocks.[1,2] This is a property which is not common to amorphous block copolymers.

Earlier studies in amorphous/crystalline block copolymers investigated the phase behavior of linear diblocks composed of polystyrene−poly(ethylene oxide) (PS−PEO),[3−6] polystyrene−poly(ϵ-caprolactone) (PS−PCL),[7] polybutadiene−poly(ϵ-caprolactone) (PB−PCL),[8] poly(butyl methacrylate)−poly(ethylene oxide) (PBMA−PEO),[9] poly(methyl methacrylate)−poly(ethylene oxide) (PMMA−PEO)[10] and in the triblocks polyϵ-caprolactone)−poly(dimethyl siloxane)−poly(ϵ-caprolactone) (PCL−PDMS−PCL)[11] and PDMS−PEO−PDMS.[12] An unusual chain folding of polyethylene (PE) has been reported in the diblock copolymers of poly(ethylene-*co*-butylene)−polyethylene[13] and in poly(vinyl cyclohexane)−polyethylene.[14] In both cases the orientation of chain-folded PE stems was parallel to the lamellar interface. The competition between microphase separation and crystallization has been investigated in poly(ethylene)−poly(ethylene-*alt*-propylene) (PE−PEP),[15] poly(ethylene)−poly(propylene) (PE/hhPP),[16] and poly(ethylene)−poly(ethylethylene) (PE−PEE).[17] In the latter study it was found that the original microphase separated morphologies were destroyed due to the PE chain folding upon crystallization. From the systems above, the PS−PEO diblock copolymer system received a lot of attention mainly because of the great block dissimilarity and incompatibility.

The extensive studies of Lotz and Kovacs[3] have shown that PS−PEO diblock copolymers form a lamellar morphology and the chain stems of the crystalline parts are perpendicular to the lamellae planes. Gervais and Gallot[4,5,7] have studied the phase behavior of several block copolymers, including PS−PEO, and found a lamellar crystalline structure at temperatures below 50 °C. PEO was found to crystallize in a double-layer folded structure and the number of folds was found to depend largely on the amorphous block. Moreover, the nature of the crystallizable block was found to influence the crystallinity and number of folds but not the double-layer structure.

The crystallization kinetics of PEO in the PS−PEO diblock copolymers have been studied by Lotz and Kovacs.[18] They found that composition exerts a strong influence on the crystal structure and nature of crystallization process. For PEO-rich diblocks a spherulitic structure was formed comprising lamellae of crystalline folded PEO segments sandwiched by the amorphous PS segments. For PS−rich diblocks the domains had a smaller size with an ill-defined morphology. A two-stage PEO crystallization occurred for such compositions: a heterogeneous nucleation at shallow supercoolings followed by homogeneous nucleation at deeper quenches. For intermediate compositions a spherulitic texture bound to the glassy PS domains was observed.

Current theories[1,2] of domain formation in amorphous/crystalline diblock copolymers predict that a chain-folded system exists under *equilibrium* conditions. This situation in block copolymers is in sharp contrast to semicrystalline homopolymers since chain folding in the homopolymer case is only metastable: long-time annealing reduces the amount of chain folds, and in the limit of infinite annealing time, an extended chain crystal structure can be formed. Theories[1,2] provide the equilibrium domain size, which is largely determined by the balance of the total energy due to chain folding in the crystalline blocks with the associated entropic conformation and stretching free energy of the amorphous blocks. There is a coupling in the energetics of the amorphous and crystalline parts which results in

† Foundation of Research and Technology-Hellas (FORTH).
‡ University of Patras and Institute of Chemical Engineering and High Temperature Chemical Processes.
[⊗] Abstract published in *Advance ACS Abstracts,* July 1, 1997.

S0024-9297(96)01611-7 CCC: $14.00

Table 1. Molecular Characteristics of the PEO and the PEO−PS−PEO Triblock Copolymers

sample	$\bar{M}_w$(LS)	$\bar{M}_w/\bar{M}_n$[a]	$\bar{M}_w$(PS)[a]	$\bar{M}_w/M_n$(PS)[a]	$\bar{M}_w$[b](PEO block)	W_{PS} (%)	X_c^{WAXS} (%)	X_c^{DSC} (%)[e]
PEO-22	22 000	1.06					64	71
ESE-1	133 000	1.19	68 000	1.09	32 500	53[c]	56	61
ESE-2	82 000	1.17	33 500	1.13	24 200	34[d]		52

[a] From GPC. [b] Calculated value from M_w (PEO block) = (M_w(COP) − M_w(PS))/2. [c] From refractive index increment. [d] From elemental analysis. [e] Using ΔH_0 = 200 J/g.

an intimate connection between their structural properties.

PS−PEO diblock copolymers have been studied extensively with respect to the morphology and crystallization kinetics of PEO with techniques such as dilatometry,[18] X-ray diffraction,[19] and optical microscopy. However, very little is known about the structure and crystallization process in PEO−PS−PEO triblock copolymers. The melt flow behavior of such triblocks has been examined.[20] The influence of annealing and casting solvent on the morphology was recently reported,[21] and the influence of the solvent quality on the chain conformation was investigated.[22] In the present work we focus on the crystallization kinetics and the crystal structure in two PEO−PS−PEO triblock copolymers which are crystallized from the ordered melt. For the structural investigation we employed wide- and small-angle X-ray scattering (SAXS, WAXS) and optical microscopy whereas for the monitoring of the crystallization process we used differential scanning calorimetry (DSC) and rheology. With DSC we find a typical nucleation and growth process for the crystallizable component. We compare the crystallization process of PEO in the triblocks with the homopolymer. There is a reduction in crystallinity and in the equilibrium melting temperature in the triblocks. Our results are in favor of a multilayer lamellar morphology of PEO with a spherulitic superstructure. Rheology is a very sensitive to the crystallization/melting process in crystallizable systems, and PEO is a sensitive probe of crystallization; thus, we explored the effect of shear on the crystallization kinetics.

Experimental Section

Materials. The PEO−PS−PEO triblock copolymers used in this work were synthesized by sequential anionic polymerization according to well-known procedures. The PS midblock was prepared first in THF at −40 °C using naphthalene potassium as the initiator. Part of the reaction solution was sampled out, and the PS precursor was isolated for characterization. A chosen amount of ethylene oxide (EO) was added subsequently and the temperature increased slowly to 30 °C. The polymerization of EO proceeded for 24 h. The triblock copolymer was recovered by precipitation into heptane, redissolved in benzene, filtered, and freeze-dried. PEO homopolymer was purchased by Polysciences Inc. All samples, the triblocks and the PS blocks were characterized by means of steric exclusion chromatography, light scattering, differential refractometry, and elemental analysis.The characterization data are given in Table 1.

Optical Microscopy. An Olympus BH-2 optical microscope fitted with crossed nicols was used for the morphology characterization. The micrographs for the triblocks were obtained in films cast in acetone. The samples were dried adequately, heated to 130 °C for 15 min, and annealed at 47 °C to complete the crystallization. The PEO homopolymer film was obtained by press-melting at 80 °C and annealed at the same temperature with the triblocks except for one sample (Figure 1a) which was crystallized at −30 °C. A filled space of spherulites was observed in all samples (Figure 1) but the number of spherulites depends both on the supercooling (i.e., Figure 1a,b) and on the particular triblock (see below).

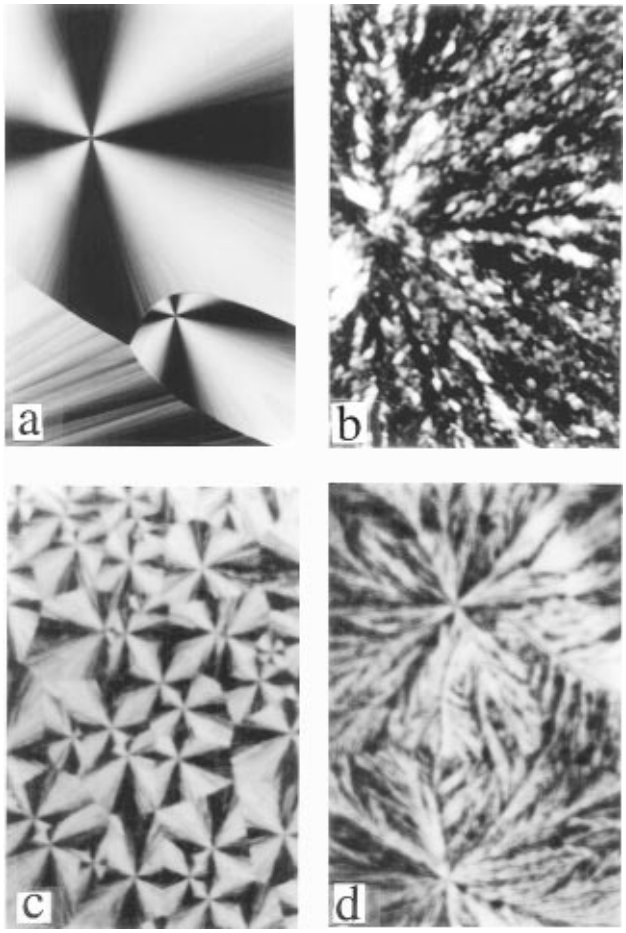

Figure 1. Polarized optical micrographs of (a) PEO crystallized from the melt at −30 °C, (b) PEO crystallized isothermally at 47 °C, and (c) ESE-2 and (d) ESE-1 both crystallized isothermally at 47 °C.

Wide- and Small-Angle X-ray Scattering. The WAXS measurements were carried out with a Siemens $\theta-\theta$ diffractomer (Model D500T) in reflection geometry. The Cu Kα radiation was used from a Siemens generator (Kristalloflex 710 H) operating at 35 kV and 30 mA and a graphite monochromator was utilized in front of the detector (λ = 0.154 nm). Measurements were made in the 2θ range from 4 to 60° with 0.01° steps. All measurements were made by heating. For PEO, profiles at the following temperatures were taken: 25, 35, 45, 55, 65, and 75 °C. The scattering profiles at the two highest temperatures are shown in Figure 2. For the triblock ESE-1 measurements were made at 25,35,45, 50, 55, and 65 °C. Again, the profiles at the two highest temperatures are shown in Figure 2. SAXS measurements were made at the X3A2 beamline of the National Synchrotron Light Source (NSLS), Brookhaven National Laboratory (BNL). A pinhole collimation system was used, and image plates were used as the detector. The sample-to-detector distance was 106 cm. The SAXS data, corrected for the background, are shown as insets to Figure 2. In the raw intensity data of PEO, the main peak at Q^* = 0.0536 nm^{-1} is followed by additional peaks at higher Q. From the Lorentz-corrected SAXS pattern (shown in Figure 2) we extract three peaks at positions 0.068, 0.27, and 0.53 nm^{-1}. The long period, i.e., the average distance of lamellar crystals separated by amorphous regions, is extracted from

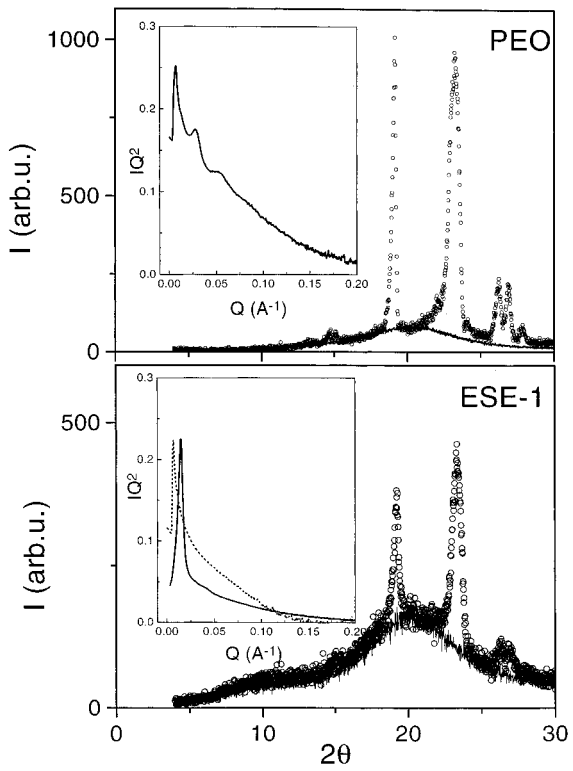

Figure 2. Wide-angle X-ray scattering intensity profiles for PEO (top) and for the triblock ESE-1 (bottom). Data were taken on heating and scattering profiles only at two temperatures are shown. Key: PEO, solid line, $T = 75$ °C, symbols, $T = 65$ °C; ESE-1, solid line, $T = 65$ °C, symbols, $T = 55$ °C. Notice the reduction in the melting temperature and the identical position of the Bragg reflections in PEO and ESE-1. In the insets, the SAXS data for PEO (top) and ESE-1 (solid line) and ESE-2 (dashed line) (bottom) are shown.

the first maximum of the Lorentz-corrected data, which when corrected for the crystallinity (Table 1) result in a PEO crystal thickness of about 65 nm. This value should be compared with the thickness of the fully extended chain crystal (integral folding (IF) = 0) l_{max} (=$(M_n^{PEO}/M_n^{EO}) \times 0.278$ nm), which is 140 nm. Therefore, the main SAXS peak corresponds to once folded chains (IF = 1). The peaks at higher Q values (with d-spacings of 23 and 12 nm) correspond to smaller PEO fractions of shorter crystals. The number of chain folds depends highly on the crystallization temperature and thermal history. For PEO with MW's in the range 6000−10000, stable once-folded chains were formed.[23]

The triblock copolymers were melt-pressed at 150 °C, where both systems are in the ordered state (see Figure 15, below) and then quenched to room temperature. The SAXS spectra (shown in Figure 2 as inset) were taken at 40 °C and show main peaks at positions 0.148 and 0.0693 nm^{-1} for ESE-1 and ESE-2, respectively, without higher order peaks, which is indicative of a rather poor microdomain ordering. The large difference in the d-spacings and the fact that the d-spacing of ESE-2 is longer than for ESE-1 cannot be accounted simply by their molar masses, reflecting that the amorphous block excerts a strong influence on the thickness of the PEO domains. This probably originates from the closeness of the T_m to the T_g of the hard phase.

Differential Scanning Calorimetry. A Polymer-Laboratories DSC was used with an integral cooling jacket capable of programmed cyclic temperature tests over the range −160 to +400 °C. A dry gas purge was used for accurate measurements near ambient temperature ranges. The isothermal kinetic experiments were made by monitoring both the exothermal and endothermal peaks. In the former experiment, samples were heated to an initial temperature of 75 °C and then cooled to different final temperatures with a cooling rate of 10 °C/min. The final temperatures were in the ranges 44−55, 41−46, and 42−52 °C for PEO, ESE-1 and ESE-2, respectively. Samples remained in the final temperatures for sufficient time to allow complete crystallization with an exotherm. After crystallization the samples were heated to the initial temperature at 10 °C/min. In the latter experiment, samples were cooled down from the initial temperature (75 °C) to some final temperatures (at 10 °C/min) where they remained for different time intervals. Subsequently, they were heated at 10 °C/min to the initial temperature, and the heats of fusion were obtained from the integration of the endothermal peaks.

Rheology. A Rheometric Scientific dynamic stress rheometer (DSR) with a controlled strain option was used to measure the storage (G') and loss (G'') moduli. A parallel-plate sample geometry was used, and the sample temperature was controlled by two electrically heated plates within the range 30−150 °C with a stability better than 0.1 K. Different experiments were performed: (i) isochronal temperature scans at $\omega = 1$ rad/s with a heating/cooling rate of 1 °C/min, (ii) isothermal frequency scans within the frequency range $10^{-1} < \omega < 10^2$ rad/s and for temperatures up to 150 °C, and (iii) isochronal/isothermal time scans at $\omega = 1$ rad/s and for different temperatures below the equilibrium melting points.

Results and Discussion

PEO. The optical micrographs of PEO (Figure 1a,b) show a spherulitic structure and in some cases (Figure 1a), more than one size of spherulites can be observed. The WAXS profiles of PEO are shown in Figure 2 and can be used to determine the melting temperature and the crystallinity X_c^{WAXS}. The crystal structure of PEO is monoclinic[24] with a unit cell parameter of 1.93 nm along the helix axis and results in the peaks in the wide-angle region shown in the figure. With increasing temperature, the structure melts at approximately 65 °C and the intense Bragg reflections disappear, revealing a featureless amorphous halo. The weight fraction of crystallinity X_c can be obtained from the area under the amorphous halo (I_a) and crystalline reflections (I_c) as

$$X_c^{WAXS} = \frac{1}{f}\left(\frac{I_c}{I_c + I_a}\right) \quad (1)$$

where f is the weight fraction of PEO. The values obtained with this procedure are depicted in Table 1. The degree of crystallinity was subsequently determined by DSC as $X_c^{DSC} = \Delta H/\Delta H_0$, where ΔH_0 refers to the heat of fusion for completely crystallized PEO (ΔH_0 = 200 J/g[25]) and is also included in Table 1.

In the following experiments we have investigated the crystallization kinetics of PEO using calorimetry and rheology. The first calorimetric experiment was made by monitoring the endothermal peak. The sample was cooled from an initial temperature $T_i = 75$ °C to a temperature below the melting point for different preset intervals of time and the heat of fusion was determined from the integrated intensity of the endothermal peak (after correcting for the additional heat capacity effect). The resulting thermograms are shown in Figure 3 for a crystallization temperature of 53 °C and for different waiting times as indicated. There is a progressive increase of ΔH_t with increasing times and a saturation for times longer than 15 min (ΔH_∞). The normalized peak area, $X = \Delta H_t/\Delta H_\infty$, is plotted in the inset and conforms to the Avrami equation[26]

$$1 - X = e^{-zt^n} \quad (2)$$

where z is the rate constant and n is a combined function of the number of dimensions in which growth

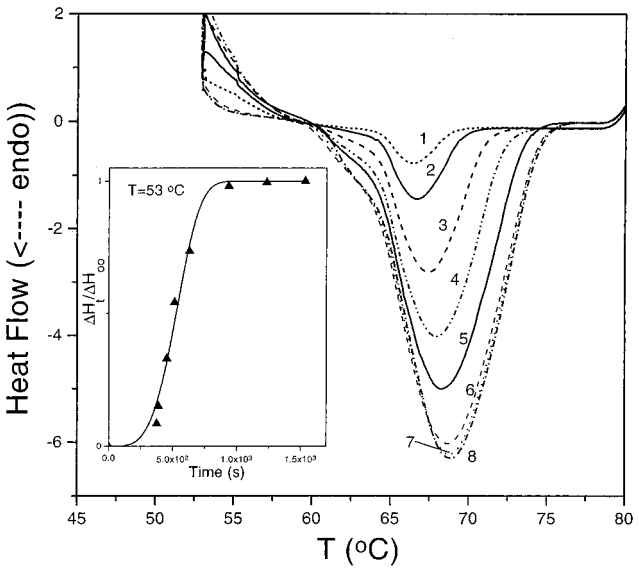

Figure 3. Crystallization kinetics of PEO obtained by DSC. The sample was first heated to 80 °C and quenched to 53 °C where it was crystallized for different time intervals: (1) 0.5 min, (2) 1 min, (3) 2 min, (4) 3 min, (5) 5 min, (6) 10 min, (7) 15 min, and (8) 20 min. The corresponding heats of fusion obtained from the integration of the endothermal peaks are plotted in the inset. The solid line represents a fit to the Avrami equation with $n = 4$.

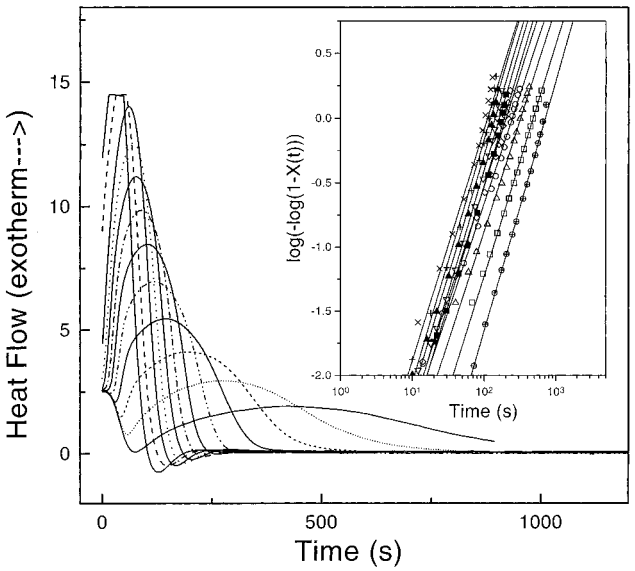

Figure 4. Isothermal crystallization of PEO obtained by DSC. The sample was first heated to 80 °C and quenched to different final temperatures in the range 44−53 °C. The inset gives a typical Avrami plot for the volume fraction of crystalline material $X(t)$ at different temperatures: (⊕) 55, (□) 54, (△) 53, (○) 52, (◇) 51, (■) 50, (▽) 49, (▲) 48, (+) 47, and (×) 46 °C. The solid lines are fits to the Avrami equation ($n = 2$).

takes place and of the time-dependence of the nucleation process (*homogeneous* vs *heterogeneous*). While the rate constant, z, provides a quantitative check on the course of crystallization, the Avrami exponent, n, provides a qualitative information on the nature of the nucleation and growth process. The case $n = 4$ can only result from spherulitic growth from sporadic nuclei (homogeneous nucleation), whereas $n = 3$ can result both from spherulitic growth of instantaneous nuclei (heterogeneous nucleation) or disklike (lamellar) growth from sporadic nuclei. The analysis involves plotting $\log(-\log(1 - X))$ as a function of $\log t$ and determining n from the slope and z from the intercept. Deviations from the Avrami analysis, that is, nonlinearities in the plot or fractional exponents, can in principle result from (i) simultaneous growth of two different types of spherulites or (ii) from a single structure obtained from growth of two types of nuclei (homogeneous *and* heterogeneous). In the present case, the enthalpy of fusion data, shown in Figure 3 as an inset, conform to the Avrami equation with $n \approx 4$, which implies spherulitic growth and homogeneous nucleation.

The second type of experiment (exothermal peak) involved isothermal crystallization following jumps from an initial temperature of 75 °C to different final crystallization temperatures. In such experiment we monitor the crystallization peak as it develops with time, and the result is shown in Figure 4. From the exothermal peak we can obtain $X(t)$ as

$$1 - X(t) = \frac{\Delta H_\infty - \Delta H_t}{\Delta H_\infty - \Delta H_0} \qquad (3)$$

where ΔH_∞ and ΔH_t are the latent heats after time t and on complete crystallization ($t = \infty$). The Avrami analysis was employed again to describe the nucleation and growth process, and the result is shown in the inset. The data for all temperatures can be well represented by straight lines with slope of 2. On the basis of the spherulitic structures observed in the optical micrographs (Figure 1), one would expect an exponent of 4 or 3. It is worth mentioning that both values can be found in published calorimetric and dilatometric data of PEO.[18,27−29] When the thermograms are taken in the exothermal mode, we observe the initial stages of crystallization before the impingement of spherulites. The growing entities during the early stages have a lamellar (or disklike) structure of folded PEO chains ($n = 2$). Alternatively, the higher exponent in the endothermal mode (reflecting melting of spherulites rather than crystallites) is accompanied by a slower rate (eq 2) as evidenced by comparing the kinetics at 53 °C (Figures 3 and 4). Lastly, the heats of fusion and crystallization are insensitive to the presence of secondary aggregates.[27]

Rheology is a very sensitive technique to the crystallization/melting processes and can be used not only to identify the T_m but also to follow the crystallization kinetics following a T-jump from the melt state. Figure 5 shows the result from an isochronal measurement of the shear modulus $|G^*|$, obtained on cooling with a rate of 1 °C/min and subsequent heating at the same rate. The abrupt increase (decrease) of $|G^*|$ indicates the crystallization (melting) of PEO. Given the large separation of the moduli in the crystal and melt states, we can study the crystallization kinetics by performing quench experiments from $T_i = 70$ °C to different temperatures of crystallization. An example of such experiment is shown in Figure 6 for $T_c = 59$ °C. For $t < 10^4$ s, $|G^*|$ exhibits a plateau with a value of 200 dyn/cm^2 also obtained in Figure 5. At $t \approx 10^4$ s, there is an abrupt increase of $|G^*|$ by 5 orders of magnitude and the process is completed within 1000 s, after which the long-time plateau is reached. The plateau values at $t < 10^4$ and $t > 10^4$ s are associated, respectively, with the supercooled melt and crystalline material. To make this more evident, we performed isothermal frequency scans at the same temperature but for the time intervals corresponding to the low and high plateaus. Such experiments are feasible in the present system since a frequency sweep from 10^{-1} to 10^2 rad/s lasts for about

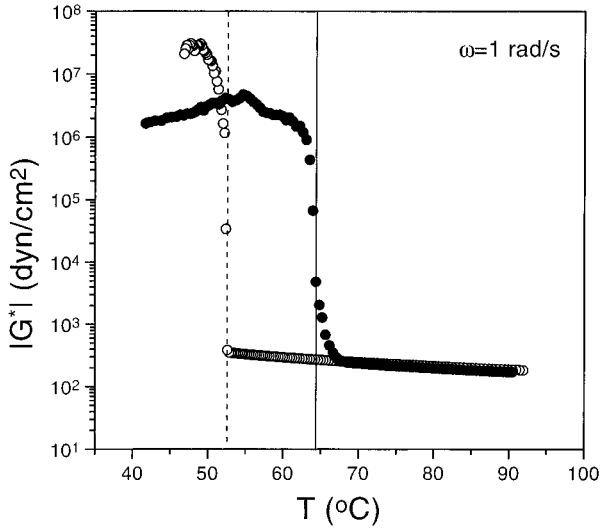

Figure 5. Isochronal measurements of the absolute value of the complex modulus G^* of PEO at 1 rad/s. Data obtained on cooling (○) and subsequent heating (●) are shown and the dashed and solid vertical lines signify the T_c and T_m, respectively.

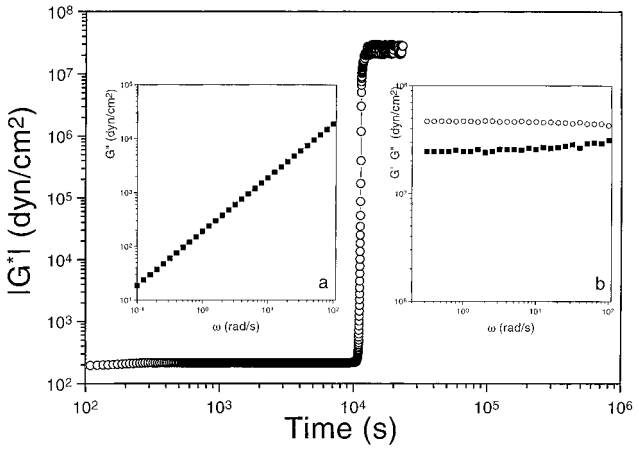

Figure 6. Isothermal crystallization of PEO at 59 °C, following a quench from 65 °C. The "liquid" and "solid" response of the system at times $t < 10^4$ and $t > 10^4$ s is shown in insets a and b, respectively.

700 s, a time much shorter than the induction and completion times. The results from such frequency scans performed at $t < 10^4$ and $t > 10^4$ s are shown as inserts to Figure 6. For the $t < 10^4$ s scan, only the loss modulus could be measured and found to display a characteristic terminal behavior ($G'' \sim \omega$) whereas for the $t > 10^4$ s both the storage (G') and loss (G'') moduli could be measured and displayed a solidlike response with only a moderate frequency dependence.

A direct comparison of the kinetic studies from DSC and rheology requires the volume fraction of the crystalline phase $\phi(t)$ from the latter experiment. To extract $\phi(t)$, the system is regarded as composed of two phases (*amorphous* and *crystalline*), the proportion of which changes with time, causing the observed changes in the dynamic mechanical response. Different models have been proposed to describe the properties of such materials. Here we are using the simplest "series" and "parallel" mechanical models which provide the limits for the mechanical response of a two-phase system as a function of the properties of the consituent components and the composition. In the "series" ("parallel") model the compliance (modulus) of the two-phase system is expressed as a linear combination of the compliances

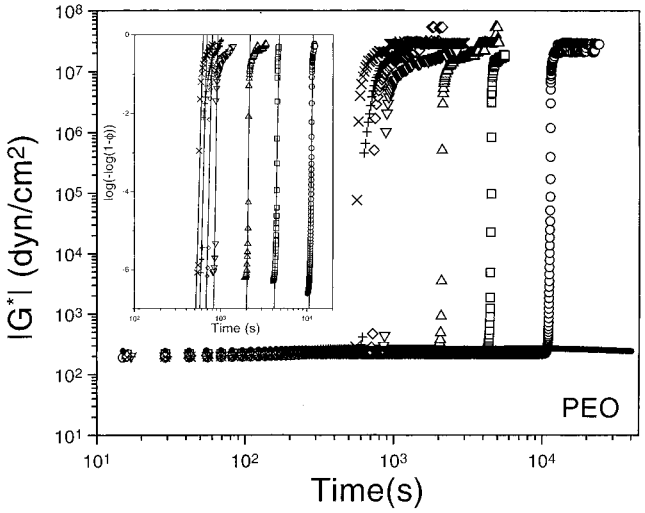

Figure 7. Isothermal crystallization of PEO. The sample was initially heated to 65 °C and quenched to different final temperatures: (●) 61, (○) 59, (□) 58, (△) 57, (▽) 56, (◇) 55, (+) 54, and (×) 53 °C. The inset gives the Avrami plots for the volume fraction of the crystalline phase $\phi(t)$, at the same temperatures.

(moduli) of the constituent phases, i.e., $J = (1 - \phi)J_0 + \phi J_\infty$, ($G = (1 - \phi)G_0 + \phi G_\infty$) where J_0 (G_0) and J_∞ (G_∞) are the compliances (moduli) of the supercooled amorphous ($t = 0$) and crystalline ($t = \infty$) phases, respectively. The time-dependences of ϕ obtained from the two models are analyzed independently by fitting to the Avrami equation (analogous to eq 2):

$$1 - \phi(t) = e^{-zt^n} \tag{4}$$

A direct comparison of $\phi(t)$ and $X(t)$ is now possible. We find that the estimated half-time of the crystallization process is similar to that found in calorimetry (see below) but the shape of the rheological process cannot be accounted by the Avrami equation. When semicrystalline polymers and glass-forming liquids are subjected to shear, they exhibit similar effects below their melting point since the smallest deformation can cause instantaneous crystallization.[30] Given that the characteristic time is not influenced by the shear we conclude that the external shear field first (for t shorter than a characteristic time $t_{1/2}$) inhibits the creation of nucleation sites, resulting in longer induction times, and then speeds up the final stages of the nucleation and growth process. Changing the crystallization temperature does not really affect the shape of $|G^*(t)|$, as shown in Figure 7. In the kinetic study shown in this figure it is interesting to note the same short- and long-time plateau values at the different crystallization temperatures. In contrast to block copolymers composed of two amorphous blocks,[31] PEO crystallization is accomplished via a single process, and this is independent of the temperature of crystallization. The result of the attempted Avrami analysis is shown in the inset and results in unreasonably high exponents ($n \approx 8$). The characteristic times, however, can be compared directly with the results of the calorimetric data. The characteristic time, $t_{1/2}$, was obtained from the Avrami analysis as $t_{1/2} = (\ln(2/z)^{1/n}$.

The comparison is made in Figure 8 where the times from calorimetry and rheology, obtained from the present study, are compared with literature data[27] on PEO crystallization, for a similar molecular weight. In the inset the shapes of the $1 - \phi(t)$ (rheology) and $1 - X(t)$

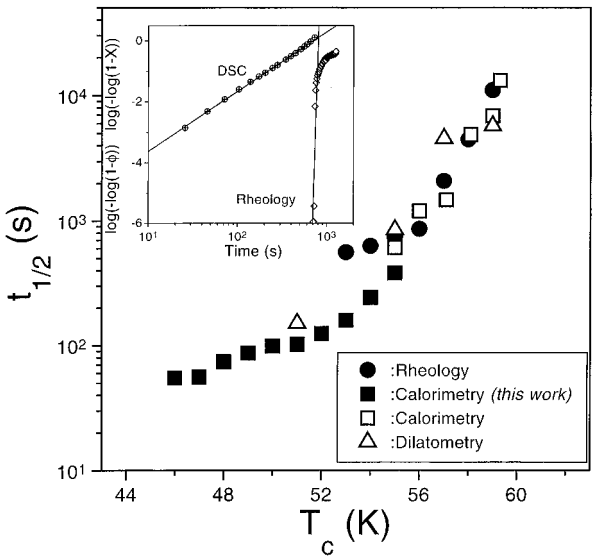

Figure 8. Half-times for the crystallization process of PEO as a function of the temperature of crystallization. Literature data[27] from calorimetry and dilatometry are also included ($M_w^{PEO} = 20\,000$).

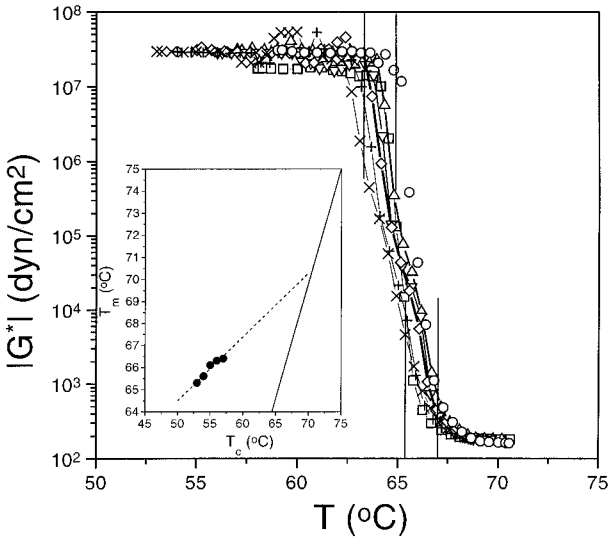

Figure 9. Isochronal measurements ($\omega = 1$ rad/s) obtained during heating following the isothermal crystallization experiments of PEO (Figure 7). The different symbols refer to the same temperatures as in Figure 7. In the inset the corresponding Hoffman−Weeks plot is shown from where the equilibrium melting point can be obtained by extrapolation.

(calorimetry) curves obtained after a quench to 55 °C are compared. Notwithstanding the different shapes of the crystallization process, the times $t_{1/2}$, from rheology and calorimetry, are in good agreement, except for the lowest temperature in the rheology data due to instrumental limitations. Following the crystallization experiments we performed heating runs in order to obtain the melting temperatures, and this is shown in Figure 9. As expected for systems which are far from equilibrium, the lower the T_c the lower the T_m, and this dependence could be used to extract the equilibrium melting point from rheology (see below). It is worth noticing, however, that the melting process occurs in two steps as indicated by the vertical lines in Figure 9, which might reflect melting of different sizes of PEO spherulites (Figure 1a). If the highest drop of the modulus is used as the signature of T_m, then the equilibrium melting temperature can be obtain by extrapolation (inset to Figure 9). It is the first time, to our knowledge that rheology is used to extract the equilibrium melting temperature of semicrystalline polymers.

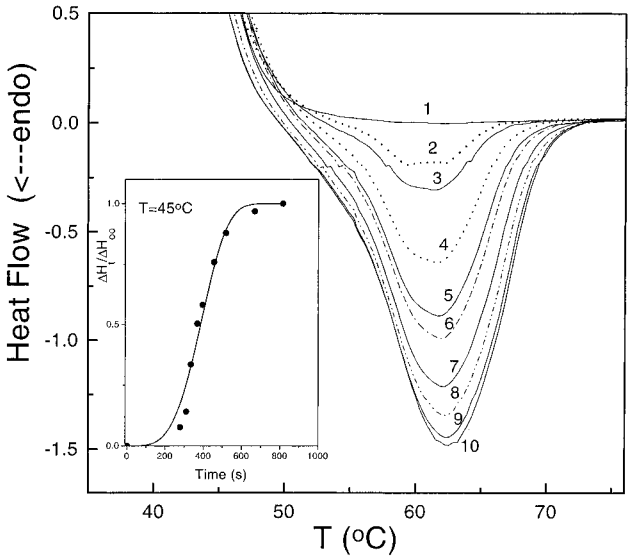

Figure 10. Crystallization kinetics of the triblock ESE-1 obtained by DSC. The sample was first heated to 70 °C and quenched to 45 °C where it crystallized for different time intervals: (1) 0.5, (2) 1, (3) 1.5, (4) 2 min, (5) 2.5, (6) 3, (7) 4, (8) 5, (9) 7.5, and (10) 10 min. The heats of fusion obtained from the endothermal peaks are plotted in the inset. The solid line is the Avrami equation with $n = 4$.

Triblock Copolymers. The WAXS profiles for the triblock copolymer ESE-1 exhibit Bragg reflections which are also observed for the PEO (Figure 2). This is indicative that PEO in the triblock copolymers crystallizes in its monoclinic form. The PS midblock does not affect the local crystal structure of the outer blocks. There are however two consequences: first the T_m is reduced (from 65 to about 55 °C) and the crystallinity as well (from 64 to 56%). A similar reduction in crystallinity was also obtained from DSC and is shown in Table 1 for the two triblock copolymers. Second, the long period in ESE-1 is much reduced compared to PEO. Isothermal kinetic experiments in the endothermal and exothermal modes were made for the triblocks as with the homopolymer. The result of the endothermal experiment for the ESE-1, following a quench from 75 °C, is shown in Figure 10. There is again a progressive increase of the heat of fusion and the results for $\Delta H_t/\Delta H_\infty$ conform to the Avrami equation (inset to Figure 10) with $n = 4$ in agreement with the homopolymer study indicating spherulitic growth from homogeneous nuclei. The results of the exothermal experiment for the same sample are shown in Figure 11 for four temperatures in the range 41−44 °C. The $X(t)$ obtained from integration of the exothermal peak conforms to the Avrami equation (inset to Figure 11) with an exponent $n \approx 2$. This situation here is reminiscent to the pure PEO case. For ESE-2 the corresponding exothermal experiments were made over the range from 52 to 58 °C and the thermograms are shown in Figure 12. An Avrami exponent of $n = 1.8 \pm 0.2$ results from the fits as shown in the inset. In conclusion, the effect of the PS midblock is mainly to reduce the crystallization/melting temperature and the crystallinity but has no effect on the local structure of PEO. However, as we will see below, both the crystallization kinetics and the crystal thickness are significantly altered in the triblocks.

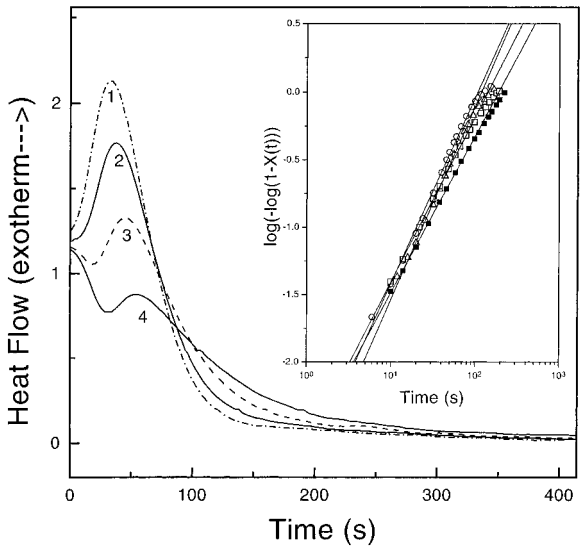

Figure 11. Isothermal crystallization of the triblock ESE-1 obtained by DSC. The sample was first heated to 70 °C and quenched to different final temperatures: (1) 41, (2) 42, (3) 43, and (4) 44 °C. The Avrami plot for the volume fraction of crystalline material is shown in the inset. Lines are fits to the Avrami equation ($n \approx 2$).

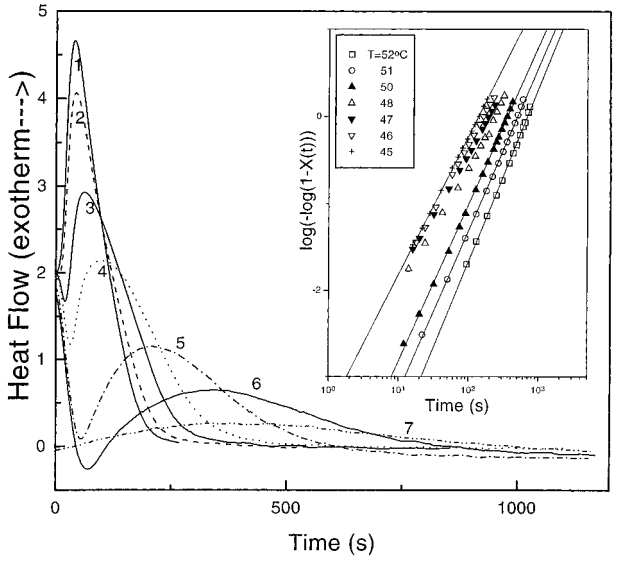

Figure 12. Isothermal crystallization of the triblock ESE-2 obtained by DSC. The sample was first heated to 70 °C and then quenched to different final temperatures: (1) 45, (2) 46, 47, (4) 48, (5) 50, (6) 51, and (7) 52 °C. The inset gives the Avrami plot for the volume fraction of crystalline material for different temperatures as indicated. The lines are fits to the Avrami equation with $n \approx 2$.

It is interesting here to compare the thermograms for the triblock and homopolymer obtained in the exothermal mode. When compared at the same T_c, the PEO crystallization in the triblock is much slower. However, this representation is misleading since this comparison should be made under conditions of equal driving force, i.e., same $\Delta T = T_m^o - T_c$, where T_m^o is the equilibrium melting temperature. This comparison requires knowledge of the equilibrium melting point in the homopolymer and the triblock copolymers. There are different ways to obtain the equilibrium melting temperature, but the most commonly used method is based on the Hoffman−Weeks analysis[32] and involves plotting the apparent melting temperature T_m' to the corresponding crystallization temperature T_c. However, a more direct way of determining T_m^o, which takes into account the

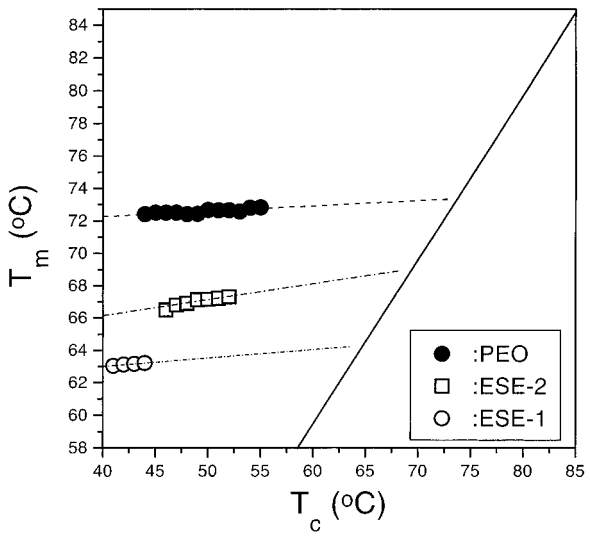

Figure 13. Hoffman−Weeks plot for PEO and for the two triblocks illustrating the decrease in T_m^o for the latter systems.

effects of lamellar thickening,[33,34] is by plotting the apparent melting temperatures vs the reciprocal lamellar thickness, obtained from SAXS. The first method is used here and therefore the T_m^o are subject to some uncertainty. For the determination of T_m^o we are using the DSC data obtained from the exothermal experiments and the result is shown in Figure 13. The solid line in the Figure indicates $T_m = T_c$. The T_m^o for each system is obtained by linear extrapolation to the $T_m = T_c$ line. The T_m^o values obtained from this analysis are 73.7, 69.5, and 65 °C for PEO, ESE-2, and ESE-1, respectively. The high T_m^o value for the homopolymer is consistent with the small number of folds ($n_f \approx 1$). A melting point depression is evidenced which is more pronounced as the amorphous PS content increases in agreement with the results from the morphological and thermal studies of PS−PEO diblock copolymers.[35−37] In general, the melting point depression implies reduction of the crystalline lamellar thickness and consequently of the spherulitic size. Indeed, a comparison of the optical micrographs of the triblocks (Figure 1c,d) show a greater number of smaller spherulites for ESE-2 which is crystallized at higher supercooling (i.e., $T_m^o - T_c = 22.5$ and 18 °C for ESE-2 and ESE-1, respectively).

The crystallization kinetics of PEO in the two tribocks and in the homopolymer can now be compared under conditions of equal supercooling (ΔT). The result is shown in Figure 14 where the characteristic time $t_{1/2}$ obtained from the Avrami analysis of the latent heats during the isothermal crystallization (exothermal peak) is plotted as a function of ΔT. According to the results shown in Figure 14, the higher the PEO molecular weight the faster the crystallization process. This is reminiscent of the nucleation and growth mechanism in amorphous diblock copolymers[38] where the ordering times scale with $N^{-1/3}$ (N is the Ginzburg parameter). In contrast, in the miscible diblock copolymer PEO−PMMA[10] containing 76% PEO, a 3-fold increase in the crystallization times was found. Such differences may result from the large differences in the thermodynamic state (i.e., interaction parameters) of the two systems.

Rheology has also been used in the triblocks aiming to identify the melting temperatures and to follow the crystallization kinetics. Isochronal temperature scans, isothermal frequency scans, and kinetic experiments were made as with the homopolymer. The results of

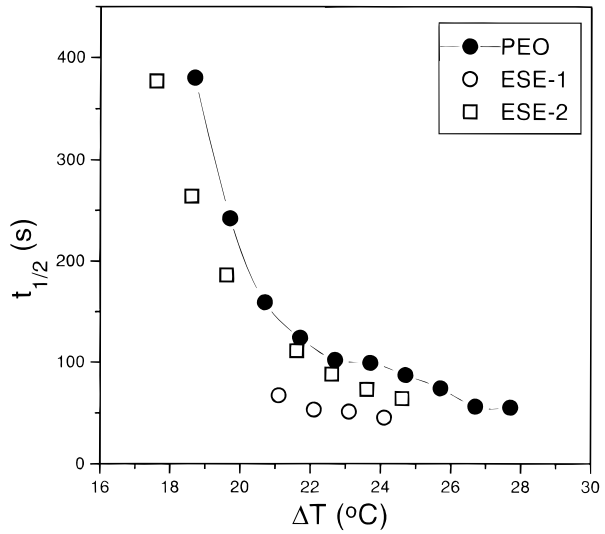

Figure 14. Crystallization times of PEO and of the two diblocks calculated from the Avrami analysis of the latent heats, obtained during the isothermal crystallization experiments and plotted vs the temperature difference from the equilibrium melting temperature ($T_m^{o,PEO}$ = 73.7 °C, $T_m^{o,ESE-2}$ = 69.5 °C, and $T_m^{o,ESE-1}$ = 65 °C).

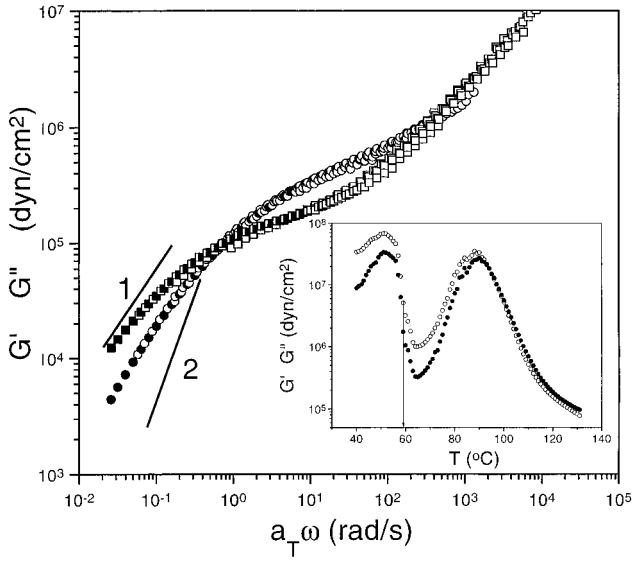

Figure 15. Isothermal frequency scans for temperatures in the range: 100−150 °C. The reference temperature was 150 °C (filled symbols). The expected slopes of G' (circles) and G'' (squares) in the terminal regime are indicated by lines. In the inset, the isochronal measurement (ω = 1 rad/s) for ESE-1, obtained during heating, is shown. The vertical arrow signifies the (reduced) T_m in the triblock copolymer.

the isothermal frequency scans are shown in Figure 15 for temperatures in the range 100−150 °C. The data for the storage and loss moduli were shifted to the corresponding data at the reference temperature (150 °C). For homogeneous copolymers, the expected slopes in the plots of log G vs log ω, in the terminal region, are 2 and 1 for G' and G'', respectively. However, even at the highest measurement temperature such values

Scheme 1

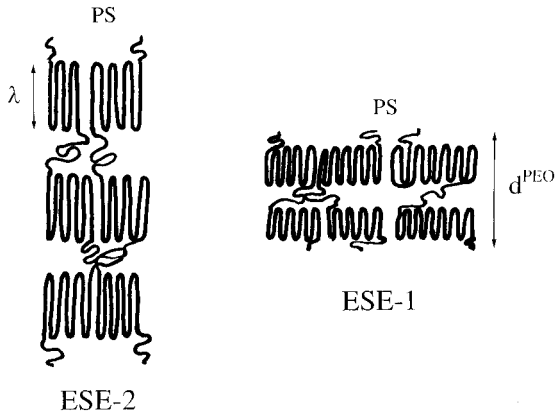

were not reached indicating on ordered structure in the melt. The result of the isochronal temperature scan (at ω = 1 rad/s) for the ESE-1 is shown in the inset to Figure 15. Both moduli are discontinuous at about 58 °C, and this signifies the T_m for the particular T_c. As with the DSC experiments, there is a reduction in the melting point in the triblocks when compared to the homopolymer (Figures 9 and 15). By a further increase of temperature both moduli develop a maximum at a temperature located in the vicinity of the PS glass transition. This signifies a large reorganization of the PS midblocks which below T_m were frustrated by the PEO lamellae. Kinetic experiments were made for the triblocks, which resulted in Avrami exponents higher than 4, as with the homopolymer. We found, however, that the short-time plateau in the modulus strongly depended on the conditions under which the initial temperature (T_i = 80 °C) was reached. This point, however, requires further investigation.

The construction of a possible structural model for the PEO crystals in the triblock copolymers is now possible. The necessary parameters are: the long period D (=$2\pi/Q^*$), the PEO domain thickness d_{PEO} (=$\varphi_{PEO}D$), the total thickness of the crystalline PEO phase $d_{c,PEO}$ (=$X_c d_{PEO}$), the thickness of the crystalline lamellar λ, and the number ν of crystalline lamellae per PEO domain (=$d_{c,PEO}/\lambda$). All parameters can be determined based on measured quantities (D, X_c, λ). For λ, the Gibbs−Thomson equation[39] is used, which relates the melting point depression from the equilibrium value to the surface free energy σ_e, and the lamellar thickness λ

$$\lambda = \frac{2\sigma_e T_m^{\,o}}{(T_m^{\,o} - T_m^{\,o\prime})\Delta H_f} \qquad (5)$$

where T_m^o and $T_m^{o\prime}$ are the equilibrium melting temperatures of PEO and of the triblocks, respectively, and $\sigma_e \approx 1.75\ \mu$J/cm^2 and $\Delta H_f \approx 260$ J/cm^3. The results for the structural parameters are summarized in Table 2 and a possible structural model is shown in Scheme 1.

The optical micrographs (Figure 1) have shown a completely space-filling spherulitic structure even for the ESE-1 (53% PS content). These results suggest that

Table 2. Structural Parameters for the PEO−PS−PEO Triblock Copolymers

sample	long period (nm)[a]	PEO-domain thickness d_{PEO} (nm)[b]	tot. thicknes of crystalline PEO phase, d_c (nm)[c]	crystalline lamellar thickness, λ (nm)[d]	no. of crystalline lamellae per PEO domain[e]
ESE-2	91	60	31	11.1	2.8
ESE-1	42.5	20	12	5.4	2.2

[a] Calculated from the SAXS peak as $D = 2\pi/Q^*$. [b] Calculated as $d_{PEO} = \varphi_{PEO}D$. [c] Calculated as $d_c = X_c^{DSC}\ d_{PEO}$. [d] From the Gibbs−Thomson eq 5. [e] Calculated as d_c/λ.

the PS amorphous phase is incorporated in the interlamellar PEO crystalline regions as has been proposed for the PEO/PMMA blends and the PS−PEO copolymers.[37,39,40] On the basis of earlier studies,[3] in constructing the model we have used a perpendicular folding of PEO to the PS−PEO interface. Notwithstanding the higher PEO molecular weight in ESE-1, the corresponding crystalline lamellar thickness is smaller than in ESE-2. Clearly, the increase in the amorphous block length from 322 units in ESE-2 to 653 units in ESE-1 significantly decreases the thickness of the crystalline layer of ESE-1. Furthermore, the number of chain folds ($n_f \sim l_{max}/\lambda - 1$) increase by a factor of 4 in going from ESE-2 to ESE-1.

This case has been treated theoretically first by DiMarzio[1] and later by Whitmore and Noolandi[2] by calculating the domain thickness in diblock copolymers where one of the components is crystalline. Both theories treated the case of incompatible blocks in a lamellar morphology and suggested that diblock copolymers form chain-folded systems under thermodynamic equilibrium. The structural properties of the amorphous and crystalline parts were found to be intimately connected as a result of the connectivity of the blocks, which imposes restrictions on the molecular conformations. In general, the lamellar thickness, λ, is controlled by two opposing factors: the energetics of the crystalline regions which drives the system toward extended chains with minimum folding (each chain fold costs energy) and the energetics of the amorphous region which favors random chains. As a result there is an equilibrium amount of chain folding in the crystalline domain. According to DiMarzio, the crystalline and amorphous lamellar thicknesses are

$$\lambda_c \approx N_c N_a^{-1/3} \tag{6}$$

$$\lambda_a \approx N_a^{2/3} \tag{7}$$

Solving the appropriate mean-field equations for the polymer chain distribution functions, Whitmore and Noolandi calculated the equilibrium domain thicknesses as

$$\lambda_c \approx N_c N_a^{-5/12} \tag{8}$$

$$\lambda_a \approx N_a^{7/12} \tag{9}$$

Furthermore, the equilibrium number of folds per chain was found to depend only on the degree of polymerization of the amorphous block ($\nu \approx N_\alpha^{5/12}$). Equations 6 and 8 predict that the amorphous block plays a significant role in determining the thickness of the crystalline layer. There is a qualitative agreement with the experimental results on the triblock copolymers (Table 2). A quantitative comparison between theory and experiment requires greater accuracy in the equilibrium melting temperatures since a small difference in the denominator of eq 5 can greatly influence the value of λ.

Conclusion

We have studied the crystallization kinetics and crystal structure of PEO in two PEO−PS−PEO triblock copolymers. A multilayer lamellar structure with a spherulitic superstructure is formed by the crystallizable block. We find that the amorphous block exerts a strong influence on the crystallization process, crystallinity, and equilibrium melting temperature and finally in the structure of PEO domains. More specifically the following points are observed.

(1) PEO in the triblock copolymers crystallizes in its usual monoclinic form, but there is a reduction in crystallinity and equilibrium melting temperature with respect to the homopolymer. As a result PEO crystals become thinner.

(2) A typical nucleation and growth mechanism exists in the triblocks as with the homopolymer, but crystallization proceeds faster in the triblocks under conditions of equal supercooling.

(3) External shear has a pronounced effect on the shape of the crystallization process but little effect on the average time.

In future studies we will investigate the dynamics in the above triblocks as well as the effect of different PS−PEO architectures on the crystal structure, morphology, and crystallization kinetics.

Acknowledgment. G.F. acknowledges the support of the Alexander von Humboldt Foundation (FOKOOP) and the Greek Secretariat of Research and Technology for a grant. We thank I. Chira for the DSC measurements and Dr. T. Pakula for stimulating discussions.

References and Notes

(1) DiMarzio, E. A.; Guttman, C. M.; Hoffman, J. D. *Macromolecules* **1980**, *13*, 1194.
(2) Whitmore, M. D.; Noolandi, J. *Macromolecules* **1988**, *21*, 1482.
(3) Lotz, B.; Kovacs, A. J.; Bassett, G. A.; Keller, A. *Kolloid Z. Z. Polym.* **1966**, *209*, 115.
(4) Gervais, M.; Gallot, B. *Makromol. Chem.* **1973**, *171*, 157; **1973**, *174*, 193; **1977**, *178*, 1577; **1977**, *178*, 2071; **1979**, *180*, 2041.
(5) Gervais, M.; Gallot, B. *Polymer* **1981**, *22*, 1124.
(6) Shimura, Y.; Hatakeyama, T. *J. Polym. Sci., Polym. Phys. Ed.* **1975**, *13*, 653.
(7) Gervais, M.; Gallot, B.; Jerome, R. Teyssie, P. *Makromol. Chem.* **1981**, *182*, 989.
(8) Nojima, S.; Kato, K.; Yamamoto, S.; Ashida, T. *Macromolecules* **1992**, *25*, 2237.
(9) Unger, R.; Beyer, D.; Donth, E. *Polymer* **1991**, *32*, 3305.
(10) Richardson, P. H.; Richards, R. W.; Blundell, D. J.; MacDonald, W. A.; Mills, P. *Polymer* **1995**, *36*, 3059.
(11) Lovinger, A. J.; Han, B. J.; Padden, F. J.; Mirau, P. A. *J. Polym. Sci., Polym. Phys. Ed* **1993**, *31*, 115.
(12) Galin, M.; Mathis, A. *Macromolecules* **1981**, *14*, 677.
(13) Douzinas, K. C.; Cohen, R. E. *Macromolecules* **1992**, *25*, 5030.
(14) Hamley, I. W.; Fairclough, J. P. A.; Ryan, A. J.; Bates, F. S.; Towns-Adrews, E. *Polymer* **1996**, *37*, 4425.
(15) Rangarajan, P.; Register, R. A.; Fetters, L. J. *Macromolecules* **1993**, *26*, 4640.
(16) Rangarajan, P.; Register, R. A.; Fetters, L. J.; Bras, W.; Naylor, S.; Ryan, A. J. *Macromolecules* **1995**, *28*, 1422.
(17) Ryan, A. J.; Hamley, I. W.; Bras, W.; Bates, F. S. *Macromolecules* **1995**, *28*, 3860.
(18) Lotz, B.; Kovacs, A. J. *Polym. Prepr. (Am. Chem. Soc., Polym. Chem. Div.)* **1969**, *10*, 820.
(19) Skoulios, A. E.; Tsouladze, G.; Franta, E. *J. Polym. Sci., Part C* **1963**, *4*, 507.
(20) Erhardt, P. F.; O'Malley, J. J.; Crystal, F. G. In *Block Copolymers*; Aggarwal, S., Ed.; Plenum Press: New York, 1970; p 195.
(21) Tsitsilianis, C.; Staikos, G.; Dondos, A.; Lutz, P.; Rempp, P. *Polymer* **1992**, *33*, 3369.
(22) Dondos, A.; Papanagopoulos, D. *J. Polym. Sci., Polym. Phys. Ed.* **1996**, *34*, 1281.
(23) Buckley, C. P.; Kovacs, A. J. *Prog. Colloid Polym. Sci.* **1975**, *58*, 44; *Colloid Polym. Sci.* **1976**, *254*, 695.
(24) Tadokoro, H.; Chatani, Y.; Yoshiharo, T.; Tamara, S.; Nurahashi, S. *Makromol. Chem.* **1974**, *73*, 109.
(25) Different values of ΔH_∞ of PEO have been reported in the literature: (a) Vidotto, G.; Levy, D.; Kovacs, A. J. *Kolloid Z. Z. Polym.* **1969**, *230*, 289 (203 J/g). (b) Van Krevelen, D. W. in *Properties of Polymers*, 2nd ed.; Elsevier: Amsterdam, 1976 (199.5 J/g).

(26) Avrami, M. J. *J. Chem. Phys.* **1939**, *7*, 1103; **1940**, *8*, 212; **1941**, *9*, 177.
(27) Godovsky, Yu.K.; Slonimsky, G. L.; Garbar, N. M. *J. Polym. Sci. Part C*, **1972**, *38*, 1.
(28) Beech, D. R.; Booth, C.; Dodgson, D. V.; Hillier, I. H. *J. Polym. Sci. A-2*, **1972**, *10*, 1555.
(29) Maclaine, J. Q. G.; Booth, C. *Polymer* **1975**, *16*, 680.
(30) Pakula, T. Private communication.
(31) Floudas, G.; Pakula, T.; Fischer, E. W.; Hadjichristidis, N.; Pispas, S. *Acta Polym.* **1994**, *45*, 176.
(32) Hoffman, J. D.; Weeks, J. J. *J. Chem. Phys.* **1965**, *42*, 4301.
(33) Mezghani, K.; Campbell, A.; Phillips, P. J. *Macromolecules* **1994**, *27*, 997.
(34) Takahashi, H.; Shibayama, M.; Hashimoto, M.; Nomura, S. *Macromolecules* **1995**, *28*, 5547.
(35) Kovacs, A.; Lotz, B. *Kolloid Z. Z. Polym.* **1966**, *209*, 97.
(36) O'Malley, J. J.; Crystal, R. G.; Erhardt P. F in *Block Copolymers*; Aggarwal, S., Ed.; Plenum Press: New York, 1970; p 163.
(37) Chow, T. S. *Macromolecules* **1990**, *23*, 333.
(38) Floudas, G.; Vlassopoulos, D.; Pitsikalis, M.; Hadjichristidis, N.; Stamm, M. *J. Chem. Phys.* **1996**, *104*, 2083.
(39) Wunderlich, B. In *Thermal Analysis*; Academic Press Inc.: San Diego, CA, 1990.
(40) Martuscelli, F.; Silvestre, C.; Addonizio, M. L.; Amelino, I. *Makromol. Chem.* **1986**, *187*, 1557.
(41) Ito, H.; Russell, T. P.; Wignall, G. D. *Macromolecules* **1987**, *20*, 2213.

MA9616118